# Inelastic neutron scattering from $UPd_2Al_3$ under high magnetic fields

E. Blackburn,[1,2,*] A. Hiess,[2] N. Bernhoeft,[3] and G. H. Lander[1]
[1]*European Commission, JRC, Institute for Transuranium Elements, Postfach 2340, Karlsruhe D-76125, Germany*
[2]*Institut Laue-Langevin, Boîte Postale 156, F-38042 Grenoble, France*
[3]*Département de Recherche Fondamentale sur la Matière Condensée, CEA-Grenoble, F-38054 Grenoble, France*
(Received 10 February 2006; revised manuscript received 29 March 2006; published 10 July 2006)

A study of the inelastic neutron scattering response of the antiferromagnetic superconductor $UPd_2Al_3$ over a wide range of external magnetic fields and temperatures is presented. We confirm that there is an inelastic pole characteristic to the superconducting state alone, and that it disappears above the superconducting critical field $B_{c2}$. Quasielastic scattering becomes apparent in fields just below $B_{c2}(T)$. At higher fields our results shed light on the normal magnetic state out of which the superconductivity develops at low fields: in the normal magnetically ordered state, the inelastic response scales as a Fermi liquid at all magnetic fields studied, with quasielastic scattering increasing significantly in the vicinity of the moment rotation transition (4.2 T at 0 K). In addition, the energy gap of a dispersive excitation present in the ordered state at all temperatures increases in an external field. At high magnetic fields, additional scattering is seen at ~4 meV energy transfer at $(0\ 0\ Q_L)$ for all $Q_L$.

DOI: 10.1103/PhysRevB.74.024406 PACS number(s): 74.70.Tx, 78.70.Nx, 71.27.+a

## I. INTRODUCTION

$UPd_2Al_3$ is an antiferromagnetic superconductor; the superconductivity develops inside the ordered magnetic phase ($T_{sc}$=1.8 K, $T_N$=14.3 K) and both phenomena are generated by the same electronic states.[1] The interplay between the magnetism and the superconductivity is a matter of lively debate, and the superconductivity in $UPd_2Al_3$ is clearly unconventional.[2] A signature of this is seen by inelastic neutron scattering at the antiferromagnetic zone center $\boldsymbol{Q}_0$ =(0 0 0.5), indicating a possible link between the antiferromagnetism and the superconductivity.[3–6]

In this paper we report on neutron inelastic scattering experiments investigating the dynamics at the antiferromagnetic zone center of $UPd_2Al_3$ as a function of applied magnetic field. The motivation was to examine how the response function changes as the superconducting state is destroyed by the external magnetic field, and then compare these changes to those already reported when the temperature is raised through $T_{sc}$.[3–6] However, this effect appears to be interwoven with field-dependent changes of the magnetization dynamics in the normal (magnetically ordered) state. We find that an external magnetic field has a significant impact on the normal state response, and this is reported in detail. To address these issues, the paper is organized into three major areas: (a) the superconducting state, (b) the normal state response at the antiferromagnetic zone center, and (c) the dispersion of the normal state response.

Figure 1 is an illustration of the hexagonal chemical unit cell for this material, which has lattice parameters $a=b$ =5.35 Å and $c$=4.185 Å in ambient conditions. In the magnetically ordered state the ferromagnetic basal planes are stacked antiferromagnetically up the $c$ axis, giving a propagation vector $\boldsymbol{q}$=[0 0 0.5]. The magnetic moment associated with each uranium site is $0.85\mu_B$.[7,8] The crystal used was that from Ref. 5, aligned to the $a^*$-$c^*$ scattering plane, with the $b$ axis vertical and parallel to the applied magnetic field. When the magnetic field is applied parallel to $c$, no transitions are observed up to the maximum field measured, 35 T.[11]

Figure 2(a) shows the phase diagram for $UPd_2Al_3$ as a function of temperature and applied magnetic field parallel to the $b$ axis (the parameter space explored in this work).[9,10] When a magnetic field is applied, $T_N$ decreases by less than 1 K, prior to a metamagnetic transition at 18 T. The gray line indicates the moment rotation illustrated in Fig. 1. In the high field phase the moments lie perpendicular to the applied field, along the $a^*$ axis pointing towards the next-nearest neighbors.

The other panels of Fig. 2 are typical inelastic responses at the antiferromagnetic zone center for the three regions of the phase diagram (paramagnetic, antiferromagnetic, and antiferromagnetic-superconducting).[3–6,12,13] The paramag-

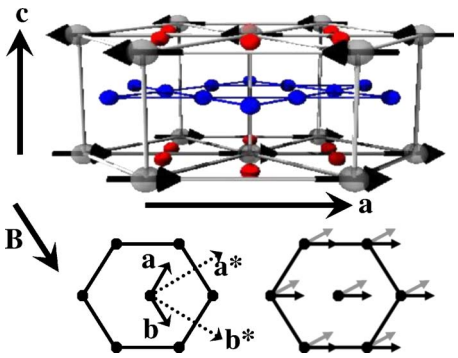


FIG. 1. (Color online) The structure of $UPd_2Al_3$. The atoms with arrows are U, the intercalating plane Al, and the remainder Pd. The arrows on the uranium ions are representations of the magnetic dipole positions and directions. The hexagons are projections of the basal plane, with the reciprocal space axes $a^*$ and $b^*$ marked as dotted lines in the left-hand hexagon. In this study, an external magnetic field $\boldsymbol{B}$ is applied parallel to the $b$ axis. The black arrows in the right-hand hexagon show one of the possible low-field magnetic domains. Above a temperature dependent applied field (see Fig. 2) the moments rotate to lie along the $a^*$ axis (the gray arrows) (Ref. 9).

 

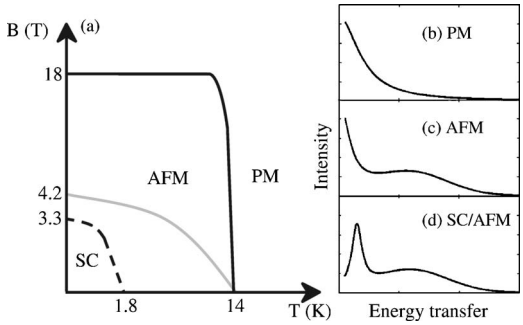


FIG. 2. (a) A schematic representation of the $(B,T)$ phase diagram for $UPd_2Al_3$ with $B\|b$, from data in Refs. 9 and 10. The dashed line denotes the onset of superconductivity inside the antiferromagnetic phase. The gray line marks the moment rotation transition illustrated in Fig. 1. At 18 T, there is a metamagnetic transition. Panels (b)–(d) are representations of the neutron inelastic response at the antiferromagnetic zone center at different points in the $(B,T)$ phase diagram. (b) is the paramagnetic response, (c) is the response of the normal antiferromagnetic state, and (d) is the response in the superconducting state.

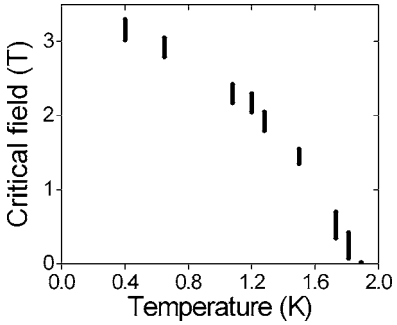


FIG. 3. Experimental $(B,T)$ phase diagram of the superconducting state in the sample of $UPd_2Al_3$ used in the neutron spectroscopy measurements, measured from the susceptibility using a mutual inductance technique. Measurements were taken by sweeping the applied magnetic field parallel to the $b$ axis at a fixed temperature. The bars indicate the full width of the anomaly observed as a function of magnetic field.

netic response consists of a single quasielastic pole, focused in momentum space around the antiferromagnetic zone centers. This has been observed out to 80 K, over five times higher than $T_N$. For descriptive purposes the normal state antiferromagnetic inelastic signal is conceptually split into a quasielastic pole and an inelastic (dispersive) response. Similarly, the signal in the antiferromagnetic-superconducting state is split into two inelastic features, one corresponding to that observed in the antiferromagnetic normal state, the other appearing at smaller energy transfer. It should be emphasized that the whole response is strongly localized in momentum space at the antiferromagnetic zone centers.

The experiments were carried out on the three-axis spectrometers IN8 and IN14 at the Institut Laue-Langevin (ILL), according to the desired energy window, in a range of sample environments. Experimental parameters are given next to the appropriate data.

## II. THE SUPERCONDUCTING STATE

### A. Experimental results

The $(B,T)$ phase diagram has been established for our sample using a mutual inductance technique inside the same 5 T cryomagnet used for the inelastic neutron scattering experiments (Fig. 3). The critical field at lowest temperatures is about 3.3 T, in accordance with the literature for a field applied perpendicular to $c$.[2]

The inelastic neutron scattering experiments were performed using the cold-neutron three-axis spectrometer IN14 at the ILL equipped with a 5 T cryomagnet. Using fixed final energy $k_f=1.15$ Å$^{-1}$ and a horizontally focusing pyrolytic graphite (PG) (002) analyzer in conjunction with a PG(002) monochromator, 60′ collimation and a Be filter in the incident beam the energy resolution was 0.06 meV half-width half-maximum (HWHM). The inelastic response at several fields and temperatures is shown in Fig. 4.

At low temperatures and low fields, a strong inelastic signal exists, centered at ~0.35 meV, in conjunction with a broader inelastic feature at higher energies. As $B_{c2}$ is approached, the low-energy inelastic feature broadens and apparently shifts to lower energies (by ~0.05 meV over 2.5 T), within the precision of the experiment, before disappearing. This is consistent with the earlier work of Metoki *et al.*[4]

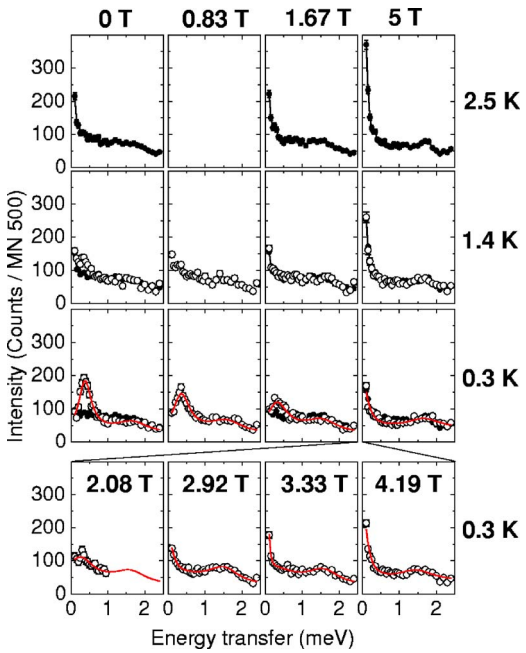


FIG. 4. (Color online) The inelastic response of $UPd_2Al_3$ at $\boldsymbol{Q}=(0\ 0\ 0.5)$ as a function of magnetic field, measured on the cold neutron three-axis spectrometer IN14 (ILL). The 2.5 K data (closed points) have been temperature scaled and overlaid with the data at 0.3 and 1.4 K at a given field to estimate the normal antiferromagnetic response as compared with the measured response (open points). The lower row of panels shows additional measurements made at 0.3 K, illustrating the disappearance of the inelastic pole associated with the superconducting state. The lines through the open points are fits described in the text.

TABLE I. The center of mass and half-width half-maximum of the low- and high-energy inelastic poles seen in the superconducting state, as obtained from fits described in the text. λ is included for completeness.

| Magnetic field (T) | Center of mass 1 (meV) | HWHM 1 (meV) | Center of mass 2 (meV) | HWHM 2 (meV) | λ (arb. units) |
|---|---|---|---|---|---|
| 0.05 | 0.35±0.01 | 0.27±0.01 | 1.70±0.05 | 0.56 | 0.04 |
| 0.42 | 0.32±0.02 | 0.31±0.01 | 1.66±0.05 | 0.56 | 0.04 |
| 0.83 | 0.32±0.01 | 0.33±0.01 | 1.63±0.05 | 0.56 | 0.04 |
| 1.25 | 0.28±0.01 | 0.33±0.01 | 1.66±0.05 | 0.56 | 0.04 |
| 1.67 | 0.27±0.02 | 0.38±0.01 | 1.59±0.05 | 0.56 | 0.04 |
| 2.08 | 0.21±0.07 | 0.45±0.15 | 1.66±0.05 | 0.56 | 0.04 |

### B. Analysis

After instrumental effects have been accounted for, the measured response gives the scattering function $S(\boldsymbol{Q},\omega)$, which is related to the imaginary part of the dynamic magnetic susceptibility $\chi$:

$$S(\boldsymbol{Q},\omega) \propto \frac{f^2(\boldsymbol{Q})}{1-\exp(-\hbar\,\omega/k_BT)}\chi''(\boldsymbol{Q},\omega,T). \qquad (1)$$

When comparing measurements made at a given $\boldsymbol{Q}$ the form factor $f^2(\boldsymbol{Q})$ can be neglected. $\chi=\chi'+i\chi''$ represents a causal process, and using the Kramers-Krönig relations $\chi''(T)=\pi\omega\chi(\omega,T)$ if $\chi(\omega,T)$ is an even function of $\omega$.[5,14]

To analyze the spectral response, a primitive model would be to split the observed dynamical susceptibility into two distinct incoherent components, $\chi=\chi_1+\chi_2$. At this level, the independent contributions can be assigned to a low, $\chi_1$, and a high energy part, $\chi_2$.[14] A mean-field coupling between the two contributions is then adopted, to give the full $5f$ neutron scattering amplitude, in an attempt to restore some of the correlations present. The (dynamical) coupling constant λ is assumed to be independent of the energy and momentum transfers observed in a given experimental setup. The two contributions are generated from the conceptual split of the total magnetization $M=M_1+M_2$ where $M_1=\chi_1(H+\lambda M_2)$ and $M_2=\chi_2(H+\lambda M_1)$. The appropriate mean-field form for the dynamic susceptibility is therefore

$$\chi=\frac{\chi_1+\chi_2+2\lambda\chi_1\chi_2}{1-\lambda^2\chi_1\chi_2}. \qquad (2)$$

The measured response of the superconducting state has been fitted using two coupled ($\lambda=0.04$) inelastic poles (treated as damped harmonic oscillators), taking into account a flat background (25 counts) and the temperature factor. The weight and width of the high-energy pole are fixed, and its center of mass allowed to vary (see Sec. III B). At the same time the weight of the low-energy pole was fixed, leaving the energy linewidth and center-of-mass as free parameters. The results of this fit are given in Table I and in Fig. 4 for $B\leq 2.08$ T at 0.3 K.

At higher fields, quasielastic scattering is clearly observable, both above and below $B_{c2}$, but is not included in the model. This might account for the apparent broadening of the low-energy inelastic pole as the field is the increased (e.g., 2.08 T at 0.3 K). The development of quasielastic scattering inside the superconducting state has previously been observed in zero field on changing the temperature.[5]

To model this, $\chi_1$ was split into a quasielastic and an inelastic part. Following Ref. 14 they were assumed to be uncoupled, with spectral weight from the inelastic part being diverted into the quasielastic portion in increasing quantities. This gives the fits illustrated in Fig. 4 at 2.92 and 3.33 T (with 43 and 51% quasielastic contribution, respectively). Fitting the data at fields ≤2.08 T does not lead to unique solutions. Finally, the values at 4.19 T and 5 T can be fitted with a 100% quasielastic contribution as if in the normal state (see Sec. III).[15]

The quasielastic contribution present at any temperature clearly increases with magnetic field. In the normal state (see, e.g., at 5 T), this increased contribution scales with temperature (see fourth column in Fig. 4). This increase appears to be a characteristic of the normal state at a given field. To investigate this further, the normal state was studied in higher fields.

## III. THE NORMAL STATE

As discussed above, the magnetic field changes the normal state properties: at 5 T and 2.5 K the quasielastic component is stronger than at zero field (first row in Fig. 4). The measurements on IN14 were therefore extended to higher fields using a 15 T cryomagnet. At fixed $k_f=1.5$ Å$^{-1}$, using a horizontally focusing PG(002) analyzer in conjunction with a PG(002) monochromator, 60′ collimation and a Be filter in the incident beam, the energy resolution was 0.1 meV HWHM.

The magnetic order described by Kita *et al.*[9] at 6 T was confirmed up to 15 T. The intensity of the Bragg peak at (0 0 0.5) is unchanged with increasing field, whereas the (1 0 0.5) reflection drops to (43±10)% of its initial intensity in the magnetic field on crossing the moment rotation transition (Fig. 2). This is consistent with the model of Kita *et al.* for which a drop to 38% is expected.

For the inelastic part of the experiment, the antiferromagnetic zone center at (1 0 0.5) was chosen for study. Changes in the low-energy (quasielastic) response are clearly observable (Fig. 5). The right-hand panel gives an overview as a function of applied magnetic field at 1.9 K. The intensity of the quasielastic response increases up to 4 T, and then decreases, becoming very broad and flat by 13 T. This decrease

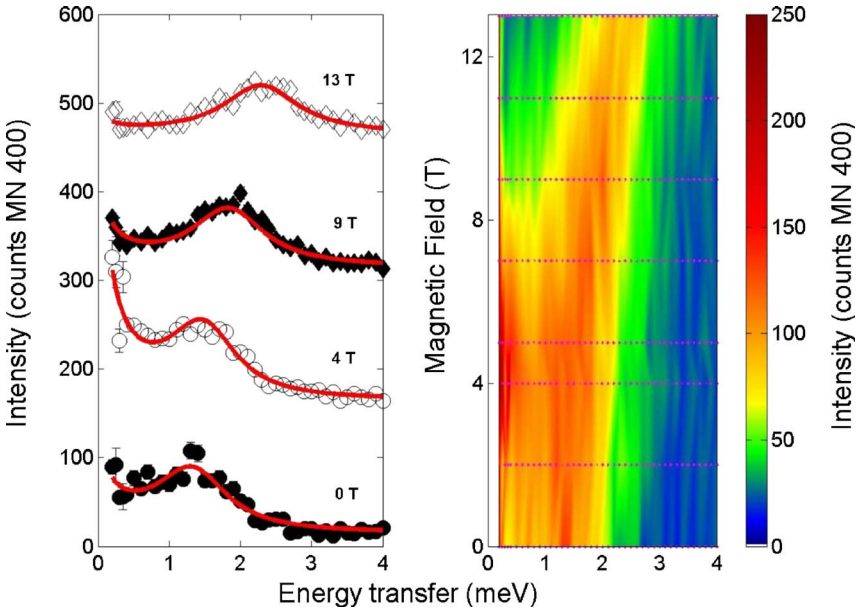


FIG. 5. (Color online) The magnetic field dependence of the inelastic response at $\boldsymbol{Q}=(1\ 0\ 0.5)$ in $UPd_2Al_3$ at 1.9 K, in the normal antiferromagnetic state, as measured on IN14 (ILL). The left-hand panel shows four individual data scans as a function of energy transfer, taken at 0, 4, 9, and 13 T. These curves are separated by 150 counts to improve visibility. The fits are described in the main text. The right-hand panel is an interpolated color plot in $(B,T)$ space, made using these (and additional) curves. Measured data points are marked by dots. The color scheme has been selected to highlight the inelastic excitation and the quasielastic response. The white space marks the resolution cutoff.

can also be seen in the high-resolution data at 0.3 K (Fig. 4) on comparing the response at 4.19 T with that at 5 T, indicating that this observation is independent of the superconducting state. The inelastic response, centered at 1.4 meV at 0 T, moves to 2.5 meV at 15 T (not shown in Fig. 5). Above 4 meV there is little change as a function of field.

Figure 6 shows similar data taken at (1 0 0.5) at $T=20$ K at 0, 4, 9, and 13 T. The signal appears purely quasielastic, with the intensity declining monotonically as a function of increasing magnetic field. Beyond 3 meV energy transfer there is no measurable field-induced difference.

At $\Delta E=0.3$ meV the momentum space width in the two accessible directions $a^*$ and $c^*$ does not change under applied magnetic field, and that of the inelastic excitation only starts to increase slightly at the highest applied fields used (above 9 T). The field and temperature induced changes at $\boldsymbol{Q}_0$ are therefore modeled solely in the energy domain.

### A. The quasielastic component of the response

In the paramagnetic regime at 20 K, the response appears to be quasielastic, and bulk measurements[1] indicate that the system has Fermi-liquid-like properties. A Langevin model, based on the time taken for the system to return to equilibrium after a random perturbation, was applied. This time is characterized by the energy linewidth $\Gamma$ of the quasielastic signal, with self-consistency enforced by setting $\Gamma=C\chi^{-1}$ where $C$ is a constant at $\boldsymbol{Q}_0$ and $\chi$ is estimated using the measured data.

To model the data, a flat background of 20 counts was added to the Langevin contribution, together with a wave-vector-independent incoherent elastic contribution (0.1 meV HWHM). The energy resolution was estimated from the incoherent elastic scattering. The parameters obtained here are therefore not comparable with those obtained in Ref. 5, where a 4D resolution ellipsoid was applied. Rather, they

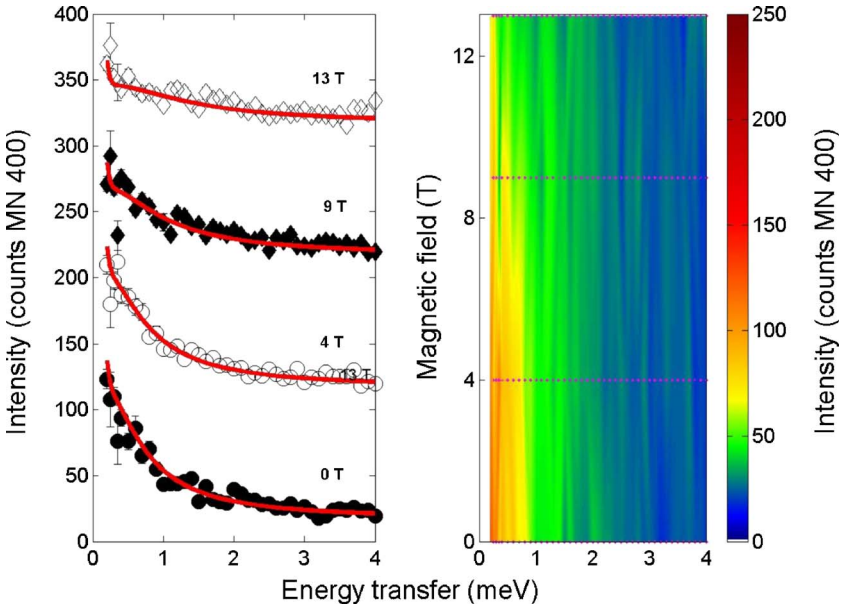


FIG. 6. (Color online) The magnetic field dependence of the inelastic response at $\boldsymbol{Q}=(1\ 0\ 0.5)$ in $UPd_2Al_3$ at 20 K, in the paramagnetic normal state, as measured on IN14 (ILL). The left-hand panel shows four individual data scans as a function of energy transfer, taken at 0, 4, 9, and 13 T. These curves are separated by 100 counts to improve visibility. The fits through these curves are described in the main text. The right-hand panel is an interpolated color plot in $(B,T)$ space, made using these curves. Measured data points are marked by dots. The color scheme matches that in Fig. 5. The white space marks the resolution cutoff.

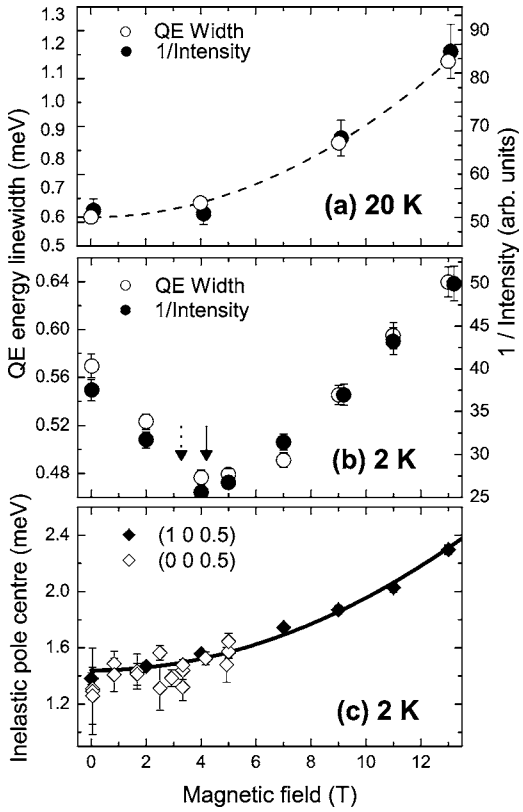


FIG. 7. The effect of applied magnetic field on the quasielastic energy half-width (open points) and the inverse intensity of the non-Bragg response (closed points) at (a) 20 and (b) 2 K. The dashed arrow in (b) indicates $B_{c2}$ (3.3 T), and the solid arrow the moment rotation transition (4.2 T). Panel (c) shows the center of the (high-energy) inelastic pole as a function of applied magnetic field at 2 K. The closed points are taken from the data shown in Fig. 5, measured at $\boldsymbol{Q}=(1\ 0\ 0.5)$. The open points are taken from (high-resolution) data illustrated in Fig. 4, measured at $\boldsymbol{Q}=(0\ 0\ 0.5)$. The lines are described in the text.

illustrate the trends in the response. For the paramagnetic state data, the fits in Fig. 6 were obtained with $C=72$ meV and a quadratic dependence of the energy linewidth $\Gamma(B)$ on the applied magnetic field ($\Gamma=\Gamma_0+\alpha B^2$ where $\Gamma_0=0.6$ meV and $\alpha=0.00319$ meV $T^{-2}$). The energy linewidth parameters are shown in Fig. 7(a).

For the antiferromagnetic state, the mean-field coupling model [Eq. (2)] is required. Assuming that the material remains Fermi-liquid-like, the linewidth $\Gamma_1$ of the quasielastic part of the response ($\chi_1$) should still obey $\Gamma=C\chi^{-1}$, but $\chi$ now includes a damped harmonic oscillator for the inelastic component $\chi_2$. A flat background of 15 counts at 1.9 K and an estimated elastic contribution were included. The value of $C$ obtained from the paramagnetic data was used. The inelastic pole $\chi_2$ was assumed to have a constant amplitude (104 arbitrary units) and half-width at half maximum (0.64 meV) over all magnetic fields, with a shifting center of mass. As the spectrometer setup had changed, the coupling constant was reevaluated, and set to $\lambda=0.042$. This value was then applied at all energy and momentum transfers studied in this setup.

The two fitted parameters (the center of mass of the inelastic pole, and the quasielastic energy linewidth) are illustrated in Fig. 7. The quasielastic energy linewidth has a minimum close to 4 T.

In Fig. 7, the energy linewidths at both 2 and 20 K are compared with the inverse intensity, as estimated by summing over the inelastic energy window measured, and correcting for background. This intensity $I$ is a crude measure of the dynamic susceptibility at $\boldsymbol{Q}_0$, and $1/I$ should be proportional to the energy linewidth. The magnetic field dependence of these two quantities is the same at both 2 and 20 K, reinforcing the reliability of the chosen model.

The behavior seen in Fig. 7(b) is reminiscent of a transition at 4 T. It therefore seems that the changes in the quasielastic linewidth (and intensity) are directly related to the moment rotation at 4.2 T (Fig. 2). As there is no change in the observed width in momentum space, the spatial correlations remain unaltered but the time correlations increase close to the moment rotation.

This model describes the data successfully and confirms that the magnetic correlation function of $UPd_2Al_3$ as measured here is consistent with Langevin (Fermi-liquid-like) behavior over a large range of the parameter space from 1.9 to 20 K and 0 to 15 T.

The near coincidence of $B_{c2}$ and the moment rotation field [Fig. 2(a)] hampers the study of the influence of an external magnetic field on the superconducting state. To resolve this issue, two possibilities present themselves. First, one might apply the external field parallel to the $b^*$ axis, as in this case, the single domain state is formed at much lower magnetic fields (0.6 T).[9] However, due to constraints imposed by the size of the sample chamber in the available cryomagnets, this would necessitate the growing of a new single crystal. A second option might be to apply a magnetic field parallel to $c$ using a horizontal cryomagnet, as in this case there are no domain reorientations. The results presented in this paper were chosen to allow direct comparison with the data of Metoki *et al.*[13] and show that the moment rotation transition has an (unanticipated) effect on the antiferromagnetic inelastic response. The effects of this transition should be considered when analyzing other (bulk) measurements.

### B. The dispersive inelastic component of the response

We now turn to the most striking feature in Fig. 5—the shift of the inelastic pole to higher energies as the magnetic field is increased [Fig. 7(c)]. The data from Fig. 5 are supplemented with high-resolution data (0.06 meV HWHM) measured at (0 0 0.5) below 5 T, although here the measured inelastic pole has less apparent intensity due to the geometrical constraints on the cross section. The origin of this inelastic feature has long been the subject of debate, and has been alternately labeled as a spin wave or as part of a magnetic exciton.

The energy gap minimum at $\boldsymbol{Q}_0$ increases monotonically with field. Cooper *et al.*[16] have developed a spin wave theory for hexagonal close-packed rare-earth metals including the effects of anisotropic exchange, axial and hexagonal anisotropy, and external magnetic fields. This can be applied to

$UPd_2Al_3$ (a case IV structure in the notation of Cooper *et al.*). In the model used, the lattice may be treated as a Bravais lattice without affecting the acoustic spin wave branch of interest.[16] Hexagonal anisotropy is necessary to give a gapped spin wave excitation. Including both the hexagonal anisotropy and a magnetic field parallel to $b$ is nontrivial; Cooper *et al.* use a modified perturbation procedure and conclude that the energy gap of the excitation should vary quadratically with the magnetic field. The line in Fig. 7(c) is a fit to a function of the form $c+aB^2$, where $B$ is the applied magnetic field. $c$ represents the effect of the hexagonal anisotropy at zero field, and places the spin wave center of mass at $1.44\pm0.05$ meV; $a=(5.2\pm0.2)\times10^{-3}$ meV $T^{-2}$.

The moment rotation does not affect the quadratic dependence of the dispersion on the magnetic field in the model described, but might affect the frequency via the hexagonal anisotropy; however, a single quadratic dependence appears to fit the data accurately. As an aside, a change in a magnetic structure like the rotation seen here is often ascribed to a "spin-flop transition." In such a transition, the spin-wave excitations develop an imaginary frequency in applied magnetic field. To stabilize the system, the magnetic structure changes. For this to occur, the frequency of the excitations would have to decrease towards 0 meV as 4 T is approached. Experimentally this is not observed, and from the theory of Cooper *et al.* it is not expected because the excitation gap increases with external field.

Finally, as mentioned above, the inelastic feature has also been attributed to a magnetic exciton developing in a crystalline electric field (CEF) scheme, with the dispersion developing through magnetic exchange, using the mechanism first developed for an anisotropic paramagnet by Becker, Fulde, and Keller.[17] The field-induced changes in the pole position of the excitation might then be brought about by (i) a decrease in the coupling between hypothetical localized and itinerant states, pulling the excitation upwards in energy, or (ii) a shift in the CEF energy level of the localized states due to the external field. Given an appropriate symmetry, this could lead to Zeeman splitting of the level, with one level eventually becoming the new ground state at ~4 T. There are several problems with this interpretation. No inelastic pole is seen in the paramagnetic state, although dispersive CEF excitations are still possible in the paramagnetic state.[17] This apparent absence could be due to significant broadening of the excitation. However, localized quasielastic scattering is still visible at 20 K, and, unlike the data at 2 K, the energy linewidth does not decrease at 4 T. This decrease would be expected even for a broadened inelastic excitation if the crystal field levels underwent Zeeman splitting.

### C. The dispersion of the inelastic response in the normal state

To complete the picture, the inelastic response away from the magnetic zone center was examined over a larger energy-transfer range, on the thermal-source three-axis spectrometer IN8. Two sets of data, sampling two different Brillouin zones, were taken at both low and high fields.

(i) For $\boldsymbol{Q}=(0\ 0\ Q_L)$ where $1.0<Q_L<1.5$ at 0 and 11.6 T using a 12 T cryomagnet. The spectrometer was operated at fixed $k_f=2.662$ Å$^{-1}$, providing optimal flux with a vertically and horizontally focusing PG(002) monochromator.

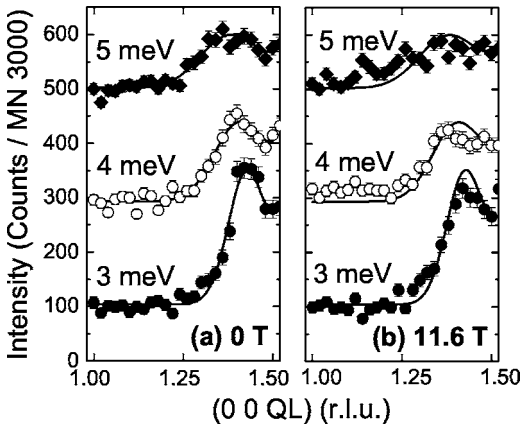


FIG. 8. Constant-energy transfer neutron spectra at 3 K in (a) 0 and (b) 11.6 T applied magnetic field. The curves are offset by 200 counts. The lines in both (a) and (b) are fits of the zero-field data in panel (a). Details are given in the text.

(ii) For $\boldsymbol{Q}=(0\ 0\ Q_L)$ where $0.5<Q_L<1.0$ at 0 and 12.5 T using a 14.9 T cryomagnet. The spectrometer was operated at fixed $k_f=2.662$ Å$^{-1}$. A vertically and horizontally focusing Si(111) monochromator was used.

In both cases, a vertically and horizontally focusing Si(111) analyzer was used, with a PG filter to suppress third-order contamination and a radial collimator along $k_f$, to cut out incoherent scattering from the aluminum window of the cryomagnets.

The inelastic response in zero field away from the magnetic zone center is given in Ref. 18. At 3 K the inelastic pole at ~1.4 meV at $\boldsymbol{Q}_0$ is well defined close to the antiferromagnetic zone center, and broadens rapidly in both momentum and energy space. Away from $\boldsymbol{Q}_0$ the momentum space width of the excitations observed seems to be more susceptible to changes in the external magnetic field. Since the scattering profile along the $c^*$ axis is simpler than that in the basal plane[14] the experiments have focused on the dispersion along $c^*$.

Some examples of the data at high and zero field are shown in Figs. 8 (constant-energy scans) and 9 (constant-$\boldsymbol{Q}$ scans). Figure 8 illustrates the steepness of the dispersion in zero field ($103\pm4$ meV Å$^{-2}$, assuming quadratic behavior), with several cuts across the inelastic excitation. The dispersion of the inelastic excitation at high applied magnetic field has a stiffness $67\pm4$ meV Å$^{-2}$. The lines in both panels are Gaussian fits of the 0 T data, assuming an excitation of equal weight on either side of the magnetic zone center. At 11.6 T, the excitation is slightly broader in momentum space, with a lower peak intensity. This may be due to the small shift upwards in energy transfer, combined with the presence of the additional scattering, broadening the excitation seen in the constant-$E$ cuts. Note that at ~4 meV, the background level appears to be higher at 11.6 T.

Figure 9 shows constant-$\boldsymbol{Q}$ scans at several positions at 0 and 11.6 T. In these cuts, the inelastic excitation is no longer clearly visible; indeed it is difficult to assign any of the features unambiguously. Nevertheless, several broad trends can be noted.

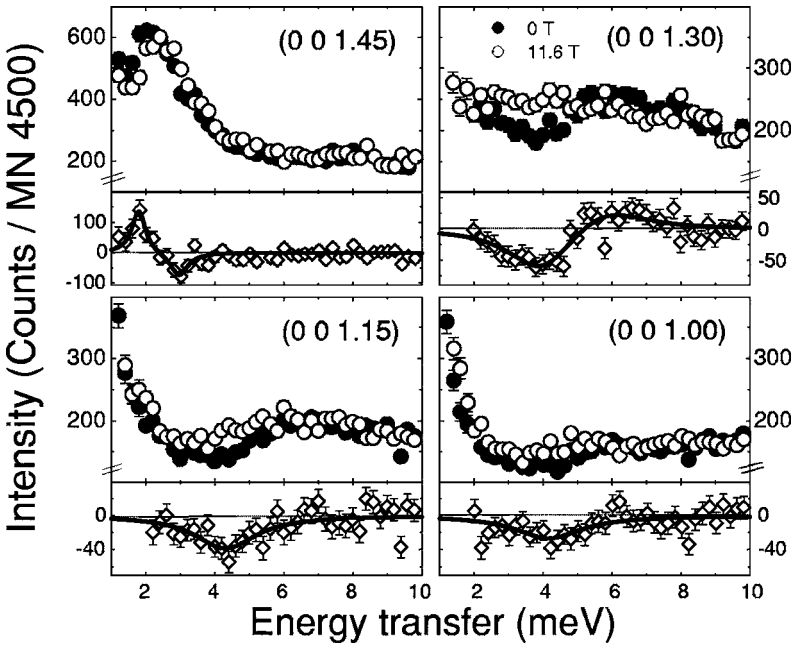


FIG. 9. Constant-$Q$ scans at 3 K at 0 T (closed points) and 11.6 T (open points). Under each scan, there is the subtraction $I_{0\ \mathrm{T}}-I_{11.6\ \mathrm{T}}$. The lines at (0 0 1.30) and (0 0 1.45) are fits of the difference between two Lorentzian line shapes representing the dispersive inelastic pole at the two fields. At (0 0 1.00) and (0 0 1.15) only one Lorentzian line shape is included in the fitting; the 0 T Lorentzian has been set to zero.

In zero field from (0 0 1.3) to (0 0 1.0) there is an increase in the observed scattering between 4 and 10 meV energy transfer, although this intensity decreases as we move away from the antiferromagnetic zone center. This appears to have evolved from the dispersive inelastic excitation. At (0 0 1.0) the boundaries of this scattering are more difficult to discern as a signal was noted at 11 meV; this has been attributed to an optic phonon, due to the intensity changes observed on changing the temperature (measured up to 120 K). Unfortunately, the instrumental background in this region could not be obtained. In the absence of this information, this scattering is assumed to be electronic in origin.

The differences between the zero- and high-field data are shown in Fig. 9. An *S*-like curve characteristic of a shift in excitation position is observed. The differences were fitted by taking the difference of two inelastic excitations at (0 0 1.45) and (0 0 1.3). At (0 0 1.15) and (0 0 1.0) the difference between the low- and high-field scans arises from an excitation in the high-field state alone.

The low-field behavior is illustrated in Fig. 10(a), where fits to the excitations are shown with the measured half width (in momentum or energy space accordingly). The filled circles represent excitations seen directly in the data, and the open circles excitations seen in the difference plots (Fig. 9). The gray ellipses represent the broad features described above.

On applying a magnetic field, there are several clear changes in the spectra (Fig. 9). The overall behavior is illustrated in Fig. 10(b), using the same conventions as in Fig. 10(a). The most notable change is the increased scattering seen at ~4 meV at (0 0 1) and (0 0 1.15) in high fields. Taking the difference of the zero- and high-field data sets picks out an excitation in the high-field state at ~4 meV energy transfer, although the signal is broad and weak (Fig. 9).

The appearance of additional scattering in a high applied magnetic field is of great interest. Several explanations are considered here.

(i) A redistribution of the broad inelastic response seen at 0 T. This is unlikely as there is no change in the scattering observed for $\Delta E>6$ meV, where the bulk of this broad response is located. In addition, the high-field excitation has a relatively well-formed (Lorentzian) line shape (Fig. 9).

(ii) The quasielastic intensity at $\boldsymbol{Q}_0$ diminishes in high fields; at 11.6 T it contains little spectral weight. If the spectral weight were redistributed throughout the zone, this would account for the lack of change in the specific heat capacity on raising the external field. Part of the spectral weight may then appear as an excited crystal field level.

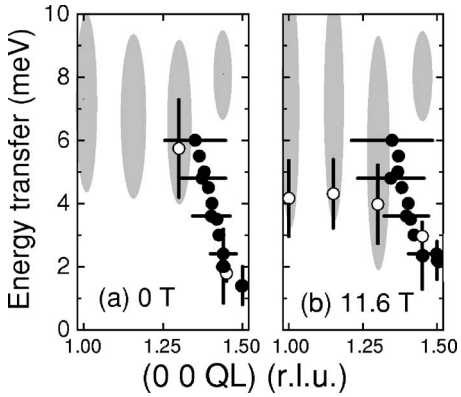


FIG. 10. Representations of the inelastic response as a function of scattering vector and energy transfer at 3 K in (a) zero field and (b) high applied magnetic field. The solid black error bars indicate the half width (in either momentum or energy space) of a peak, as determined by fitting data similar to that seen in Figs. 8 and 9. The bars shown are representative; for a given point the width can be found by extrapolation. The closed points were taken directly from data, and the open points from comparisons of the zero- and high-field data. Some of the measurements were made in a different Brillouin zone, and have been mapped appropriately. The gray ellipses correspond to intensity maxima, measured from one estimated minimum to another.

As only two field points have been measured, it is not known if the development of this feature is gradual or abrupt.

## IV. SUMMARY AND CONCLUSIONS

A series of neutron inelastic scattering experiments has been carried out on a single crystal of $UPd_2Al_3$. The original objective was to study in detail how the magnetic response at the antiferromagnetic zone center $\boldsymbol{Q}_0$ changed in an external magnetic field, in particular on passing through $B_{c2}$. One reason for doing this was to ascertain whether or not the response function behaved in the same way as when the superconductivity is quenched by heating through $T_{sc}$, studied in earlier work.[3–6] It is clear that the inelastic response at $\sim$0.35 meV that appears below $T_{sc}$ is no longer present above $B_{c2}$, and that quasielastic scattering is seen inside the superconducting state (Fig. 4). However, our understanding of the evolution of this quasielastic scattering is hampered by apparent changes in the magnetization dynamics of the system. As the external field is increased, the low-energy scattering ($<$0.5 meV) appears to increase, reaching a maximum at $\sim$4.2 T (Fig. 5), and then decreases monotonically. Based on the analysis in this paper, we believe that the increase in the quasielastic scattering arises from dynamics associated with the rotation of the moments, and *not* from the loss of superconductivity.

The normal antiferromagnetic and paramagnetic states were found to display Fermi-liquid-like behavior in external magnetic fields up to 13 T. The external magnetic field also leads to a shift in the excitation gap of the "high-energy" inelastic pole of the form expected from spin-wave theory [Fig. 7(c)]. Away from the magnetic zone center, a broad, weak response is seen along the [001] direction in the Brillouin zone at zero field as well as in high field. In high fields, an additional response is seen at 4 meV, and possible origins for this response are discussed.

## ACKNOWLEDGMENTS

The authors would like to thank Noriaki Sato of Nagoya University, Japan, for providing the sample and Jean-Louis Ragazzoni for his assistance with the dilution inserts and the magnetic susceptibility measurements. One of the authors (E.B.) would like to thank the European Commission for support in the frame of the "Training and Mobility of Researchers" programme.

*Present address: Department of Physics, University of California, San Diego, 9500 Gilman Drive, La Jolla, California 92093-0319.

[1] C. Geibel, U. Ahlheim, G. Weber, and F. Steglich, Z. Phys. B: Condens. Matter **84**, 1 (1991).
[2] T. Watanabe, K. Izawa, Y. Kasahara, Y. Haga, Y. Onuki, P. Thalmeier, K. Maki, and Y. Matsuda, Phys. Rev. B **70**, 184502 (2004).
[3] N. K. Sato, N. Aso, G. H. Lander, B. Roessli, T. Komatsubara, and Y. Endoh, J. Phys. Soc. Jpn. **66**, 1884 (1997).
[4] N. Metoki, Y. Haga, Y. Koike, and Y. Onuki, Phys. Rev. Lett. **80**, 5417 (1998).
[5] N. Bernhoeft, N. Sato, B. Roessli, N. Aso, A. Hiess, G. H. Lander, Y. Endoh, and T. Komatsubara, Phys. Rev. Lett. **81**, 4244 (1998).
[6] N. K. Sato, N. Aso, K. Miyake, R. Shiina, P. Thalmeier, G. Varelogiannis, C. Geibel, F. Steglich, P. Fulde, and T. Komatsubara, Nature (London) **410**, 340 (2001).
[7] A. Krimmel, P. Fischer, B. Roessli, H. Maletta, C. Geibel, C. Schank, A. Grauel, A. Loidl, and F. Steglich, Z. Phys. B: Condens. Matter **86**, 161 (1992).
[8] L. Paolasini, J. A. Paixao, G. H. Lander, A. Delapalme, N. K. Sato, and T. Komatsubara, J. Phys.: Condens. Matter **5**, 8905 (1993).
[9] H. Kita, A. Dönni, Y. Endoh, K. Kakurai, N. K. Sato, and T. Komatsubara, J. Phys. Soc. Jpn. **63**, 726 (1994).
[10] I. H. Hagmusa, J. C. P. Klaasse, E. Brück, A. A. Menovsky, and F. R. de Boer, Physica B **246-247**, 464 (1998).
[11] A. de Visser, H. Nakotte, L. Tai, S. A. M. Mentink, G. Nieuwenhuys, and J. Mydosh, Physica B **179**, 84 (1992).
[12] T. Petersen, T. Mason, G. Aeppli, A. Ramirez, E. Bucher, and R. Kleiman, Physica B **199-200**, 151 (1994).
[13] N. Metoki, Y. Haga, Y. Koike, N. Aso, and Y. Onuki, J. Phys. Soc. Jpn. **66**, 2560 (1997).
[14] N. Bernhoeft, Eur. Phys. J. B **13**, 685 (2000).
[15] The constant used in the fitting is not the same as that used in Sec. III.
[16] B. R. Cooper, R. J. Elliott, S. J. Nettel, and H. Suhl, Phys. Rev. **127**, 57 (1962).
[17] K. W. Becker, P. Fulde, and J. Keller, Z. Phys. B **28**, 9 (1977).
[18] A. Hiess, N. Bernhoeft, N. Metoki, G. H. Lander, B. Roessli, N. K. Sato, N. Aso, Y. Haga, Y. Koike, T. Komatsubara, and Y. Onuki, J. Phys.: Condens. Matter **18**, R437 (2006).